Journal of Solid State Electrochemistry (2019) 23:1513–1522
https://doi.org/10.1007/s10008-019-04246-0

ORIGINAL PAPER

Design and synthesis of sandwich-like $CoNi_2S_4$@C@NiCo-LDH microspheres for supercapacitors

Juan Xu[1,2] · Huada Cao[1] · Chaoying Ni[2] · Yan Wang[1] · Jianyu Cao[1] · Zhidong Chen[1]

Received: 29 November 2018 / Revised: 5 March 2019 / Accepted: 18 March 2019 / Published online: 27 March 2019

Abstract

Novel sandwich-like hollow nickel cobalt sulfides@carbon@nickel cobalt double hydroxides ($CoNi_2S_4$@C@NiCo-LDH) are synthesized using a facile microwave-assisted hydrothermal method and investigated as promising electrode materials for supercapacitors. The in-between highly conductive carbon layer simultaneously serves as uniform cover for $CoNi_2S_4$ and large-area support for ultrathin NiCo-LDH, which can restrain the microstructure change during the cyclic charge-discharge process and enhance the transmission rate of electrons and electrolyte ions. The especially nanostructured $CoNi_2S_4$@C@NiCo-LDH nanocomposites exhibit outstanding supercapacitive performances including excellent gravimetric specific capacitance (1183 mAh g^{-1} at 1 A g^{-1}) and high rate capability (85.8% retention rate at 20 A g^{-1}). More importantly, the assembled $CoNi_2S_4$@C@NiCo-LDH//graphene asymmetric supercapacitor can deliver a superhigh specific capacitance of 550 mAh g^{-1} at 1 A g^{-1}, prominent energy density of 111.9 Wh kg^{-1} and long cycling stability with 93.8% of its initial capacitance after 10,000 cycles at 5 A g^{-1}.

Keywords Sandwich-like structure · Supercapacitors · $CoNi_2S_4$@C@NiCo-LDH

Introduction

With the gradually worsening environmental issues and rising demand for clean energy, the rapid development of efficient and sustainable power storage and conversion devices needs to be further promoted. Among them, supercapacitors are rendered as special and advanced electric apparatuses with higher power density, shorter charging-discharging time and longer cycling life as compared to conventional batteries, but their energy densities, cyclic stability, and capacitance retention rates are still very low [1]. In order to increase the energy density, numerous efforts were devoted to the synthesis of novel supercapacitive electrode materials with high specific capacitance and operation voltage. To further promote the cycle stability and capacitance retention rate at high discharge current density, many hybrid nanocomposites with special nanostructure were designed.

According to energy storage mechanism at the electrode/electrolyte interface, supercapacitive electrode materials can be divided into carbonaceous nanomaterials for double-layer capacitors and redox electroactive materials for pseudocapacitors. Comparatively speaking, nanoporous carbon materials show higher rate capability, wider potential window, and longer cycle lifespan, while redox electrode materials deliver a superior gram-specific capacitance [2]. More than that, the combination of carbon nanomaterials with redox electroactive materials can bring out higher electrochemical performances than any single electrode nanomaterials because every component's distinct characteristics and functionality can be effectively integrated and fully utilized [3, 4]. In addition, some well-designed nanostructures of electrode materials can effectively endure structural deformation in the successive charge-discharge process, which is essential to long cycle life. Specially, ternary carbon-based nanohybrids have higher electrochemical specific capacitance and wider potential range than conventional binary nanocomposites [5–9]. On the other hand, as fully proved in recent literatures, the nanostructure

✉ Jianyu Cao
jyucao@hotmail.com

✉ Zhidong Chen
cjytion3@163.com

[1] School of Petrochemical Engineering, Advanced Catalysis and Green Manufacturing Collaborative Innovation Center, Changzhou University, Changzhou 213164, China

[2] Department of Materials Science and Engineering, University of Delaware, Newark 19716, USA

design plays a crucial role in the electrochemical performances of electroactive materials, and the special sandwich-like microstructure can bring about distinguished supercapacitive behaviors, including specific capacitance and rate capability [10]. For these reasons, the creative design and construction of novel multi-component ternary carbon-based hybrids with sandwich-like nanostructure for supercapacitor were put forward in this work.

Nickel cobalt sulfide ($CoNi_2S_4$) has very promising and diverse application prospect as active electrode materials in the supercapacitor field because of its larger theoretical specific capacitance and 100 times higher electrical conductivity than conventional nickel cobalt oxide ($CoNi_2O_4$) [11, 12]. However, pristine $CoNi_2S_4$ still suffers from low actual specific capacitance (less than 1800 F g^{-1}), short cycling life and fast reduced rate capability since it has low electrical conductivity and could be easily agglomerated after multiple cyclic charge-discharge process [13–16]. Thus, many high-performance carbon-based $CoNi_2S_4$ electrode materials have been thoroughly investigated by designing special architectures and combining with highly conductive matrix [7, 17–20]. For example, Wang's group prepared $CoNi_2S_4$/CNTs by one-pot solvothermal route with an ultrahigh specific capacitance of 2080 F g^{-1} at 1 A g^{-1} and a good rate capability of 61% [7]. Furthermore, graphene supported $CoNi_2S_4$ nanocomposites displayed a high specific capacitance of 2009.1 F g^{-1} at 1 A g^{-1} with a capacitance retention rate of 78.7% at 5 A g^{-1} [19]. Peng et al. reported that $CoNi_2S_4$ nanosheets were uniformly grown on the RGO sheets, which presents an extremely high specific capacitance of 1161 F g^{-1} at 5 A g^{-1} [20]. In addition, flower-like $CoNi_2S_4$/CNTs was designed and showed a good specific capacitance of 2094 F g^{-1} at 1 A g^{-1} with 72% capacity retention at 10 A g^{-1} [21]. Although combining $CoNi_2S_4$ with highly electrically conductive carbon is an achievable way and the $CoNi_2S_4$/carbon hybrids are promising electroactive nanomaterials, their rate capability, specific capacitance and cyclability still remains poor owing to the gradual degradation in nanostructure and limited electric conductivity during the charge-discharge process. Furthermore, for these carbon-supported $CoNi_2S_4$ nanocomposites, only one side of the nanoporous carbon was utilized and the induced strain encouraged the agglomeration and separation of $CoNi_2S_4$ from carbon substrate. Here, novel sandwich-like ternary $CoNi_2S_4$@C@NiCo-LDH was designed and synthesized using a facile microwave method. The carbon layer embedded between $CoNi_2S_4$ and NiCo-LDH can not only effectively accelerate the transportation of electrons and electrolyte ions, but also enhance their utilization ratio, electrical conductivity, and surface area. Furthermore, NiCo-LDHs have been regarded as a promising class of electrode materials for high-performance supercapacitors due to their higher electrochemical activity and electrical conductivity than mono-metal hydroxide [22–25].

Experimental

Reagents and materials

All the reagents were directly utilized without further purification. Commercial $Ni(NO_3)_2{\cdot}6H_2O$, $Co(NO_3)_2{\cdot}6H_2O$, glycerol, isopropanol, ethanol, thioacetamide, tris(hydroxymethyl) aminomethane, dopamine, and urea were purchased from Sinopharm Chemical Reagent Co. Ltd. in China. All aqueous solutions were freshly prepared with high purity water.

Synthesis of hollow $CoNi_2S_4$ spheres

Hollow $CoNi_2S_4$ spheres were synthesized according to a well-established hydrothermal process [26] with some modifications. Firstly, 0.182 g $Ni(NO_3)_2{\cdot}6H_2O$, 0.091 g $Co(NO_3)_2{\cdot}6H_2O$, and 20 ml glycerol were orderly added into 100 ml isopropanol. Secondly, the above-formed transparent pink solution was transferred to a Teflon-lined autoclave and then was irradiated in a Milestone Microsynth Microwave oven (Germany) for 60 min at 180 °C. After cooling, centrifuging, and washing, the generated brown NiCo-glycerate precursor was vacuum-dried at 60 °C for 12 h and then uniformly dispersed in 40 ml ethanol via a vigorous ultrasonic process. Thirdly, 160 mg thioacetamide was added into the above solution, and the obtained mixture was kept under microwave-assisted hydrothermal treatment at 160 °C for 60 min. Finally, the precipitate was centrifuged and washed, and then hollow $CoNi_2S_4$ spheres were produced.

Synthesis of core-shell nanostructured $CoNi_2S_4$@C microspheres

The 0.08 g as-prepared $CoNi_2S_4$ hollow spheres were dispersed in 25 ml 10 mmol L^{-1} tris(hydroxymethyl) aminomethane solution under vigorous stirring. After adding 80 mg dopamine, the above mixture was continuously stirred for 20 h. Subsequently, the obtained product was collected by centrifugation at 10,000 rpm and then washed with water and ethanol for three times. After being vacuum dried at 60 °C for 12 h, the synthesized precursor was heated from room temperature to 500 °C with a heating rate of 3 °C min^{-1} and maintained for 3 h under N_2 atmosphere.

Synthesis of sandwich-like $CoNi_2S_4$@C@NiCo-LDH microspheres

Sandwich-like $CoNi_2S_4$@C@NiCo-LDH microspheres were synthesized by microwave-assisted hydrothermal method. In a typical synthesis, 0.874 g $Ni(NO_3)_2{\cdot}6H_2O$, 0.437 g $Co(NO_3)_2{\cdot}6H_2O$, and 1.442 g urea were dissolved in 60 mL deionized water via an ultrasonic dispersion to form a homogeneous solution. After 0.02 g $CoNi_2S_4$@C was added, the

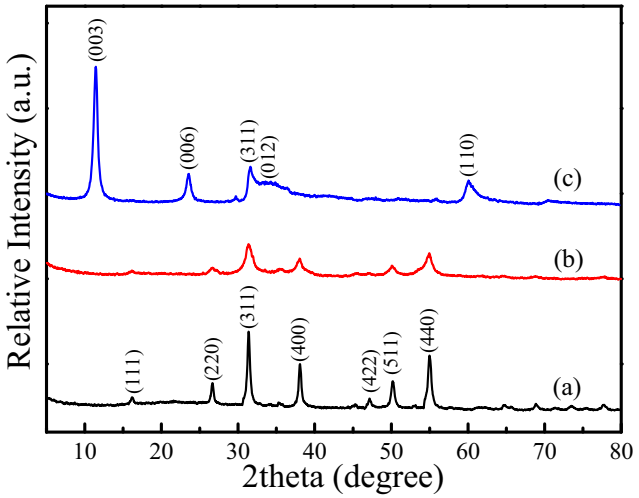

Fig. 1 XRD patterns of $CoNi_2S_4$ (a), $CoNi_2S_4$@C (b), and $CoNi_2S_4$@C@NiCo-LDH (c)

above mixture was put in a Milestone Microsynth Microwave oven (Germany) and heated for 60 min at 120 °C. The produced precipitate was separated by centrifugation at 10,000 rpm and washing with distilled water several times. After being vacuum dried at 60 °C for 12 h, $CoNi_2S_4$@C@NiCo-LDH microspheres were produced.

Characterization techniques

XRD data of the as-prepared samples were obtained from a Rigaku D/max 2500 PC diffractometer with Cu Kα radiation. The microstructures and morphology of the $CoNi_2S_4$@C@NiCo-LDH materials were observed using field-emission scanning electron microscope (FESEM, S4800, Hitachi) and transmission electron microscope (TEM, Philips Tecnai G2F20), respectively. The specific surface areas and porosity properties of the products were evaluated via a Micromeritics ASAP 2010 Brunauer-Emmett-Teller (BET) surface analyzer. The element composition was further determined by X-ray photoelectron spectroscopy (XPS, Thermo ESCALAB 250) and energy-dispersive X-ray spectrometry (EDS) that was combined with FESEM.

Preparation of working electrode and electrochemical measurements

In the preparation process of working electrode, the $CoNi_2S_4$@C@NiCo-LDH nanocomposites as electroactive materials, the acetylene black as a conductive agent, and the polytetrafluoroethylene (PTFE) as a binder were thoroughly mixed with a mass ratio of 85:20:5. After being uniformly spread on foam nickel (1 cm × 1 cm), the mazarine clay electrode was then dried at 60 °C for 12 h and pressed under 10-MPa pressure. For comparison, the $CoNi_2S_4$ and $CoNi_2S_4$@C electrodes were prepared with the same process.

In order to further evaluate the electrochemical performances of the $CoNi_2S_4$@C@NiCo-LDH electrode, electrochemical tests, including cyclic voltammetry (CV) and galvanostatic charge-discharge (GCD) were carried out in both three-electrode and two-electrode system at 25 °C by using a Versa STAT3 electrochemical workstation (Princeton Applied Research, USA). Moreover, 6 mol L^{-1} KOH aqueous solution was chosen as electrolyte. In the three-electrode system, the $CoNi_2S_4$@C@NiCo-LDH, Pt sheet, and Hg/HgO electrodes were used as the working, counter, and reference

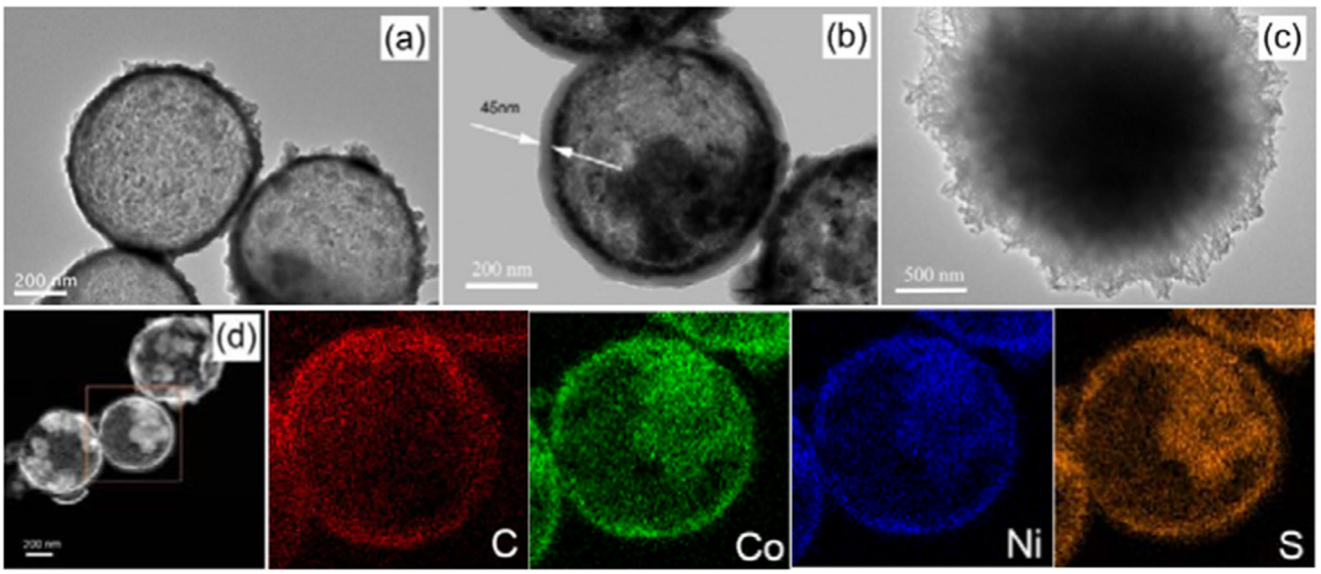

Fig. 2 TEM images of $CoNi_2S_4$ (**a**), $CoNi_2S_4$@C (**b**), $CoNi_2S_4$@C@NiCo-LDH (**c**), and elemental mapping of $CoNi_2S_4$@C (**d**)

electrodes, respectively. In the case of the designed asymmetric capacitor, graphene electrode was chosen as anode electrode. The $CoNi_2S_4$@C@NiCo-LDH cathode and the graphene anode were pressed together and separated by a porous nonwoven fabric separator. For excellent electrochemical performances, the mass proportion of cathode and anode was elaborately optimized to ensure charge balance between two electrodes [19]. The operation voltage of the $CoNi_2S_4$@C@NiCo-LDH//graphene asymmetric capacitor was set in the range of 0 to 1.4 V. Moreover, the energy density (E) and power density (P) were calculated based on the galvanostatic discharge curves by the following equation [27–29]: $E = \frac{1}{7.2}CV^2$ and $P = \frac{E}{t} * 3600$, where C (F g^{-1}), V (V), and t (s) are the specific capacitance of the assembled asymmetric capacitor, the voltage response range, and the discharge time, respectively.

Results and discussion

Structure and morphology analysis

Figure 1 shows XRD patterns of pristine $CoNi_2S_4$, $CoNi_2S_4$@C, and $CoNi_2S_4$@C@NiCo-LDH, respectively. The characteristic peaks of the pristine $CoNi_2S_4$ material that located at 16.28°, 26.67°, 31.48°, 38.18°, 50.25°, and 55.00° were assigned to the (111), (220), (311), (400), (511), and (440) planes of the spinel phase (JCPDS No. 24-0334) (curve a) [19]. For the $CoNi_2S_4$@C sample, the diffraction peaks of the $CoNi_2S_4$ became much weaker and broader (curve b), which can be ascribed to the wrapping of carbon shell on the surface of $CoNi_2S_4$. The characteristic peak of carbon at 26° cannot be clearly differentiated from the peak of $CoNi_2S_4$ because their position is very close. In the case of the $CoNi_2S_4$@C@NiCo-LDH sample, the diffraction peaks

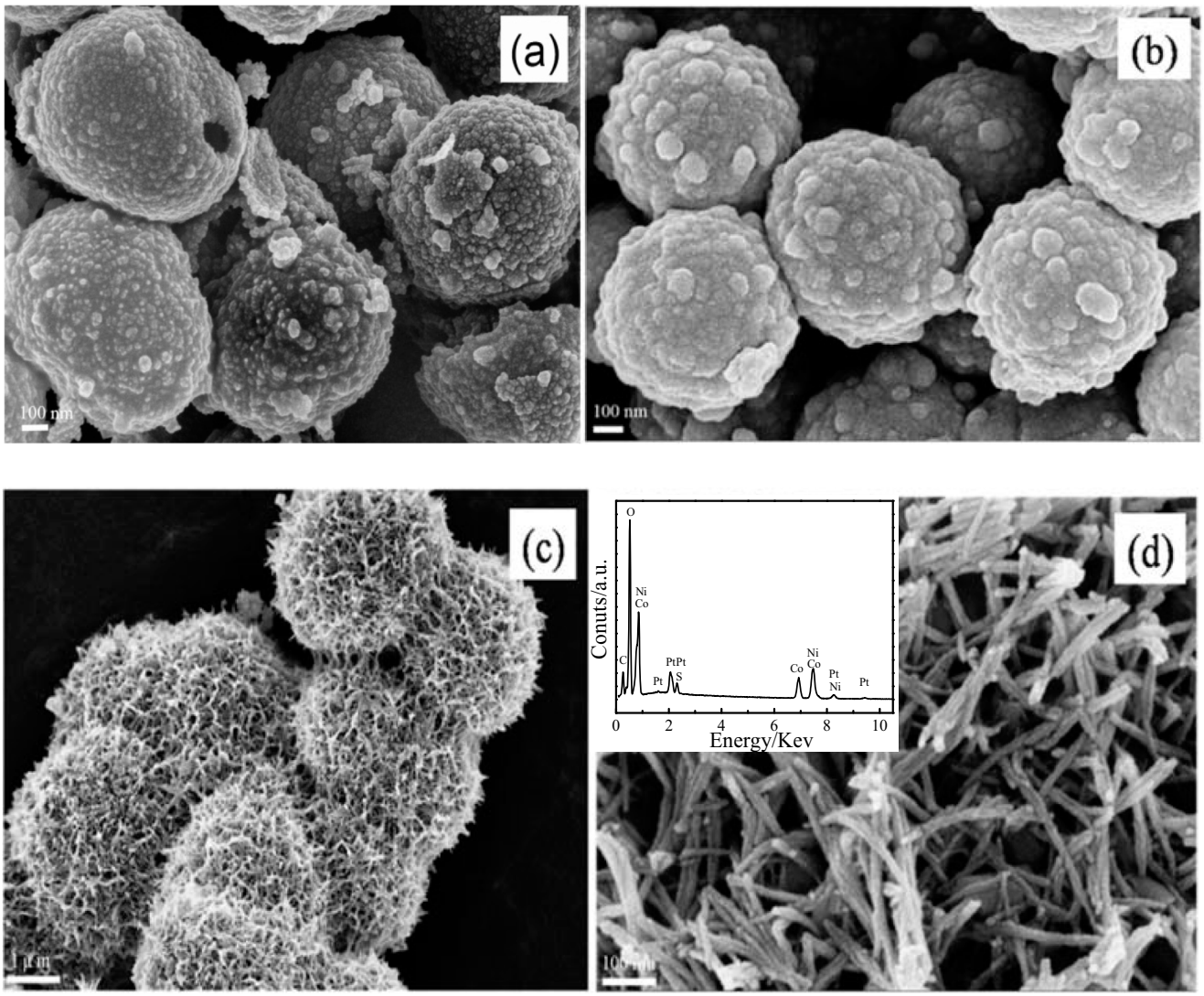

Fig. 3 FESEM images of $CoNi_2S_4$ (**a**), $CoNi_2S_4$@C (**b**), and $CoNi_2S_4$@C@NiCo-LDH (**c**, **d**). The corresponding EDS pattern of $CoNi_2S_4$@C@NiCo-LDH was illustrated in the inset.

match well with the standard α-$Ni(OH)_2$ (JCPDS No. 38-0715) and α-$Co(OH)_2$ (JCPDS No. 46-0605). Furthermore, the diffraction peak intensity of $CoNi_2S_4$ became too weak to be observed except the strongest peak at (311) plane, implying that the surface of $CoNi_2S_4$@C was closely wrapped by NiCo-LDH (curve c).

The morphology and microstructure of the $CoNi_2S_4$, $CoNi_2S_4$@C, and $CoNi_2S_4$@C@NiCo-LDH were characterized by TEM, as shown in Fig. 2. Pristine $CoNi_2S_4$ displayed a homogeneous hollow spherical nanostructure, and its average diameter is ca. 700 nm (Fig. 2a). For the $CoNi_2S_4$@C sample, obvious core-shell nanospheres were observed after the wrapping of carbon and the carbon shell spacing is ca. 45 nm (Fig. 2b). After the coating of NiCo-LDH, the surface of $CoNi_2S_4$@C was uniformly wrapped with a thick layer of hairy litchi shell and the diameter of the $CoNi_2S_4$@C@NiCo-LDH sample is increased to ca. 2.7 μm (Fig. 2c). The structure nature of the $CoNi_2S_4$@C can be ascertained by element mapping images (Fig. 2d), which illustrated that C, Co, Ni, and S were evenly distributed. Particularly, obvious carbon shell nanostructure was obtained from the carbon mapping image. As reported in literatures [30, 31], the pores or holes of unique core-shell architecture can act as effective transportation channels for the electrolyte ions during charge-discharge process. Meanwhile, coarse and nanoporous structure can bring about large surface area, which helps to the fast electron transfer and diffusion of electrolyte ions into the underneath part of the $CoNi_2S_4$@C@NiCo-LDH sample. Furthermore, the highly conductive carbon layer embedded between $CoNi_2S_4$ and NiCo-LDH also can enhance the transfer rate of electrons. Thus, much more active sites can take part in the electrochemical reaction and higher specific capacitance can be obtained. In summary, the coarse and nanoporous structure helps to the increase in surface area and transfer rate of electrons and electrolyte ions.

Figure 3 shows the FESEM images of the $CoNi_2S_4$, $CoNi_2S_4$@C, and $CoNi_2S_4$@C@NiCo-LDH sample and the corresponding EDS pattern of the $CoNi_2S_4$@C@ NiCo-LDH. As observed, the pristine $NiCo_2S_4$ hollow spheres are quite uniform and the surfaces are composed with tiny nanoparticles (Fig. 3a). After the polymerization and carbonation of dopamine, the surface of $CoNi_2S_4$ was coated with rough carbon shell (Fig. 3b). In the case of the $CoNi_2S_4$@C@NiCo-LDH sample, their surface shows fluffy pompon morphology (Fig. 3c). A magnified FESEM image displays that the villiform surface is composed of many tiny nanoribbons (Fig. 3d). The inserted EDS data further proved that the $CoNi_2S_4$@C@NiCo-LDH nanocomposite was mainly composed of Ni, Co, S, C, and O elements, in well agreement with the elemental mapping results of TEM. The existence of Pt comes from the plating process for the FESEM determination.

Figure 4 presents the nitrogen adsorption-desorption isotherms and pore size distribution plots of the $CoNi_2S_4$,

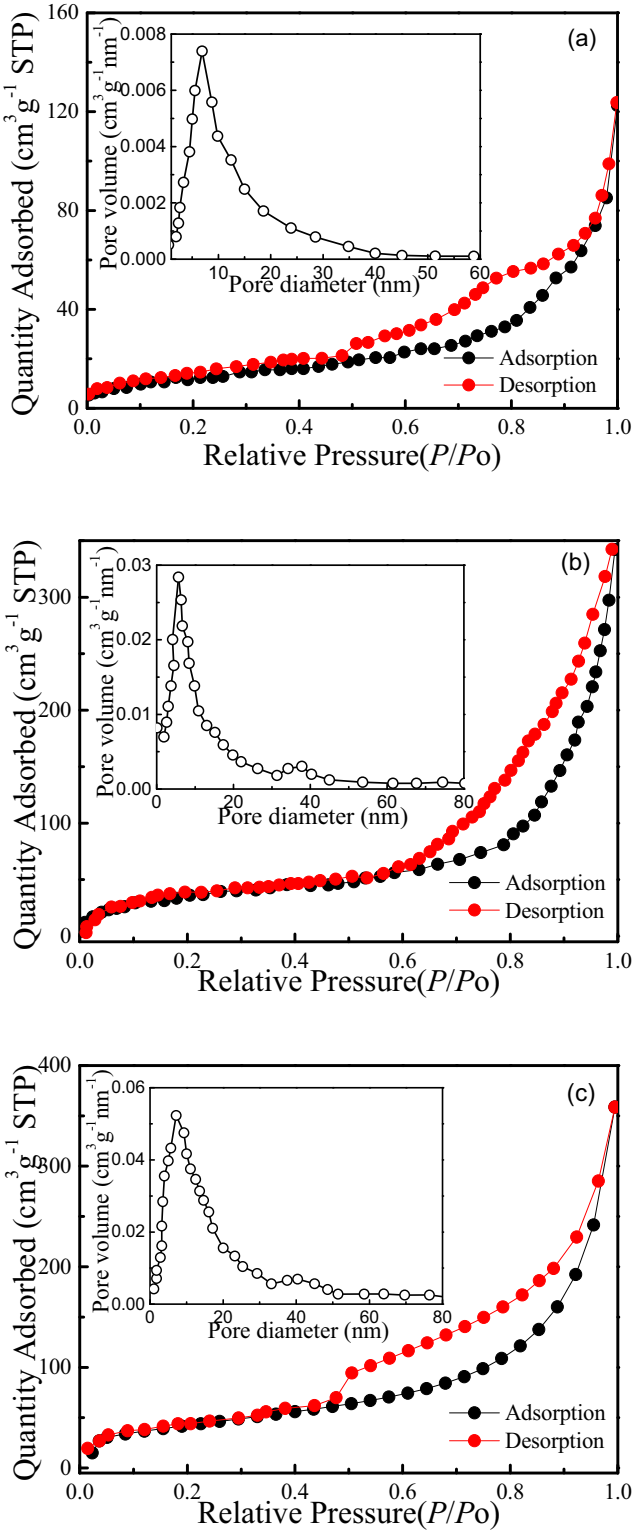

Fig. 4 N_2 adsorption-desorption isotherm curves of $CoNi_2S_4$ (**a**), $CoNi_2S_4$@C (**b**), and $CoNi_2S_4$@C@NiCo-LDH (**c**). Their corresponding pore size distribution plots for the as-prepared samples were presented in the inset.

Table 1 BET properties of as-prepared samples

Sample	S_{BET} (m^2 g^{-1})	V_{pore} (cm^3 g^{-1})	d_{BJH} (nm)
$CoNi_2S_4$	68.6	0.08	7.8
$CoNi_2S_4$@C	169.2	0.36	8.7
$CoNi_2S_4$@C@NiCo-LDH	235.6	0.68	12.9

$CoNi_2S_4$@C, and $CoNi_2S_4$@C@NiCo-LDH. The structural properties of these three samples are summarized in Table 1. For all the three samples, typical IV isotherm with a H_2-type hysteresis loop in the nitrogen desorption branch at a high P/P_0 relative pressure appeared, manifesting a porous nanostructure [32]. By comparison, the hysteresis loop of $CoNi_2S_4$@C@NiCo-LDH appears at lower pressure, indicating the existence of much more macropores and mesopores. As listed in Table 1, the $CoNi_2S_4$@C@NiCo-LDH sample has the largest BET specific surface area and pore volume, which is very helpful to the increase in electrochemical performances.

The elemental composition and valence state of the $CoNi_2S_4$@C@NiCo-LDH nanocomposite were further evaluated using XPS techniques, as shown in Fig. 5. Survey XPS spectra reveal that the as-prepared $CoNi_2S_4$@C@NiCo-LDH mainly contains Ni, Co, C, O, and S elements (Fig. 5a). Moreover, the fitted Ni 2p and Co 2p peaks can be respectively divided into two spin-

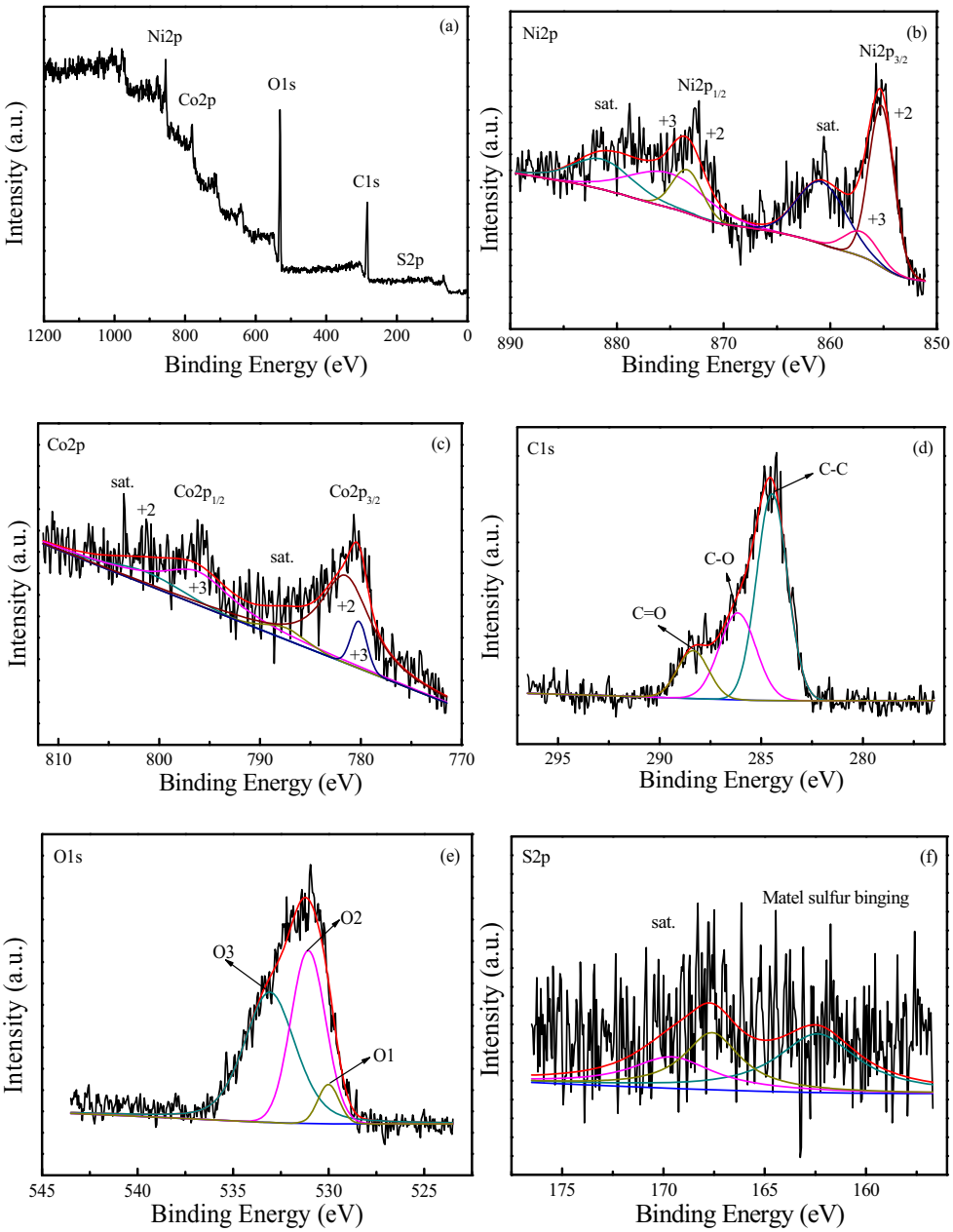

Fig. 5 Survey XPS spectra of $CoNi_2S_4$@C@NiCo-LDH sample (**a**), the corresponding Ni 2p (**b**), Co 2p (**c**), C 1s (**d**), O 1s (**e**), and S 2p (**f**) peaks

orbit doublets and two shakeup satellites (Sat.). For the Ni 2p spectra (Fig. 5b), the peaks at 855.3 and 873.4 eV are ascribed to Ni^{2+} and the peaks at 857.1 and 875.2 eV are assigned to Ni^{3+} [16]. With regard to the Co 2p spectra, two pairs of separate peaks can be obviously observed (Fig. 5c). One pair of peaks was located at 780.2 eV and 796.2 eV, corresponding to Co $2p_{3/2}$ and Co $2p_{1/2}$ of Co^{2+}. The other couple of peaks at 781.5 eV and 801.2 eV are typical of Co^{3+} [33]. In the case of C1s spectra, the peaks situated at 284.5, 286.2, and 288.4 eV are attributed to the C–C, C–O, and C=O bonds (Fig. 5d), respectively [33]. The O 1s spectra were fitted into three discrete peaks at 530.0, 531.1, and 533.0 eV (Fig. 5e), which can be attributed to M–O–M, M–O–H, and H–O–H [34]. As for the S 2p spectra, two main peaks and one shake-up satellite appeared (Fig. 5f). The main peak at 162.4 eV is characteristic of metal-sulfur bonds, while the main peak at 167.7 eV belongs to sulfur ions [19].

Electrochemical performances of the $CoNi_2S_4$@C@NiCo-LDH microspheres

Figure 6 presents cyclic voltammetry (CV) and galvanostatic charge-discharge (GCD) curves of pristine $CoNi_2S_4$, $CoNi_2S_4$@C, and $CoNi_2S_4$@C@NiCo-LDH electrodes in a three-electrode system. For all of the three electrodes, each of the CV curves has a pair of redox peaks during the scanning process (Fig. 6A), illustrating that their electrochemical performances in alkaline electrolyte belong to Faradaic pseudocapacitive behaviors. After the coating of carbon shell on the surface of $CoNi_2S_4$, the potential difference value between the oxidation peak and reduction peak decreased,

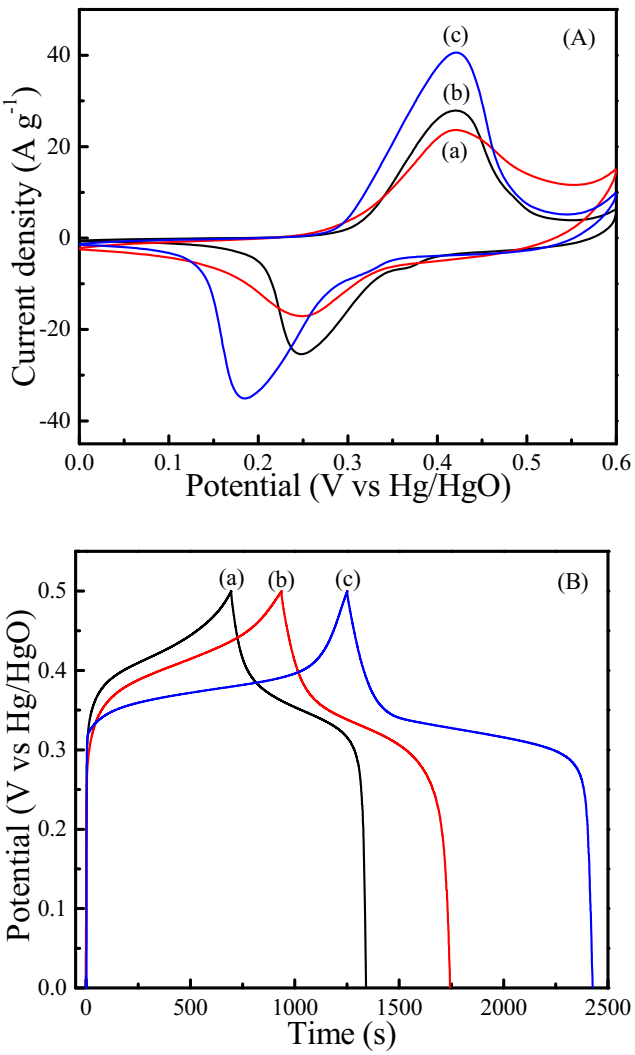

Fig. 6 Comparison of CV (**A**) and charge-discharge (**B**) curves of the $CoNi_2S_4$ (a), $CoNi_2S_4$@C (b), and $CoNi_2S_4$@C@NiCo-LDH electrodes (c). The scan rate and current density were set as 5 mV s^{-1} and 1 A g^{-1}, respectively.

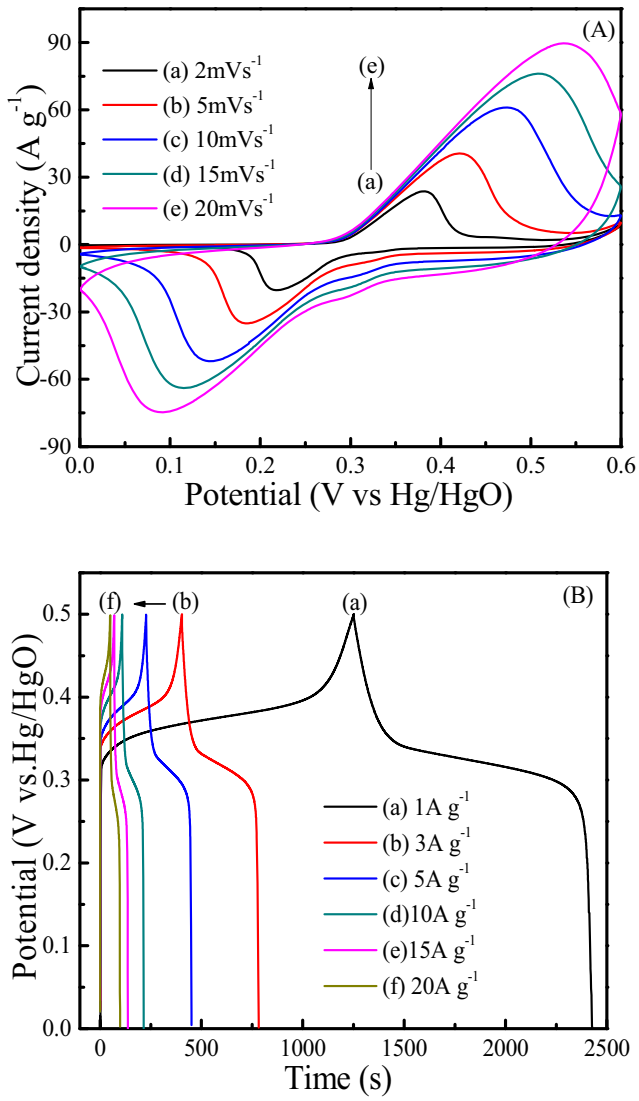

Fig. 7 CV (**A**) and charge-discharge curves (**B**) of the $CoNi_2S_4$@C@NiCo-LDH electrode at various scan rates and current densities

indicating more excellent electrochemical reversibility. In contrast, the $CoNi_2S_4$@C@NiCo-LDH electrode has the largest integral area and highest redox current intensity than that of the pristine $CoNi_2S_4$ and $CoNi_2S_4$@C electrode, proving the best electrochemical capacitances [35]. Based on the quasi-symmetric galvanostatic charge-discharge curves at 1 A g^{-1} (Fig. 6B), the specific capacitances of $CoNi_2S_4$, $CoNi_2S_4$@C, and $CoNi_2S_4$@C@NiCo-LDH electrodes have been calculated as 683, 876, and 1183 mAh g^{-1}, which further confirms the result of CV test. The increase in specific capacitance may come from the special sandwich nanostructure and the synergetic effect of $CoNi_2S_4$ supporting, carbon coating, and NiCo-LDH modification [36].

Figure 7 reveals CV and charge-discharge curves of the $CoNi_2S_4$@C@NiCo-LDH electrode at multiple scan rates and current densities. The redox peak current densities and potential differences gradually increase with the raise of scan rates and charge-discharge current densities (Fig. 7A), indicating that the $CoNi_2S_4$@C@NiCo-LDH electrode has fast charge-discharge response [37] and the redox electrochemical reaction was mainly limited by the charge transfer kinetics [38]. To further explore rate capacitive performances, charge-discharge measurements were executed with a potential window of 0~0.5 V at successively increased current densities from 1 to 20 A g^{-1} (Fig. 7B). Based on the discharge time, the specific capacitances of the pristine $CoNi_2S_4$@C@NiCo-LDH electrode can attain 1183, 1153, 1141, 1119, 1078, and 1015 mAh g^{-1} at multiple discharge current densities of 1, 3, 5, 10, 15, and 20 A g^{-1}, respectively. Even at a high current density of 20 A g^{-1}, the capacitance retention rate still can retain 85.8% of its initial capacitance, exhibiting better rate capability than reported NiCo-LDH and carbon/NiCo-LDH [24, 39]. The excellent capacitance retention value of the $CoNi_2S_4$@C@NiCo-LDH electrode may come from the highly electroconductive carbon layer that embedded between $CoNi_2S_4$ and NiCo-LDH, which efficiently enhanced the transfer of electrons and electrolyte ions.

Electrochemical properties of the assembled $CoNi_2S_4$@C@NiCo-LDH//graphene asymmetric supercapacitor

To sufficiently investigate the performances of sandwich nanostructured $CoNi_2S_4$@C@NiCo-LDH in practical electrochemical devices, an asymmetric supercapacitor was fabricated using the $CoNi_2S_4$@C@NiCo-LDH as cathode and commercial graphene as anode. Figure 8 displays the CV, charge-discharge, Ragone, and cyclic stability curves of the as-designed $CoNi_2S_4$@C@NiCo-LDH//graphene asymmetric supercapacitor at different scan rates and current densities. As illustrated, the current densities of the $CoNi_2S_4$@C@NiCo-LDH//graphene asymmetric supercapacitor increased with the elevation of scan rates and the CV curves were composed of two disparate parts: a narrow quasi-rectangular shape at 0~0.6 V and a broad redox peak at 0.6~1.4 V (Fig. 8A), proving that the specific capacitance comes from the combinatorial capacitance of electrical double layer and faradaic reaction. Besides, even if the current density

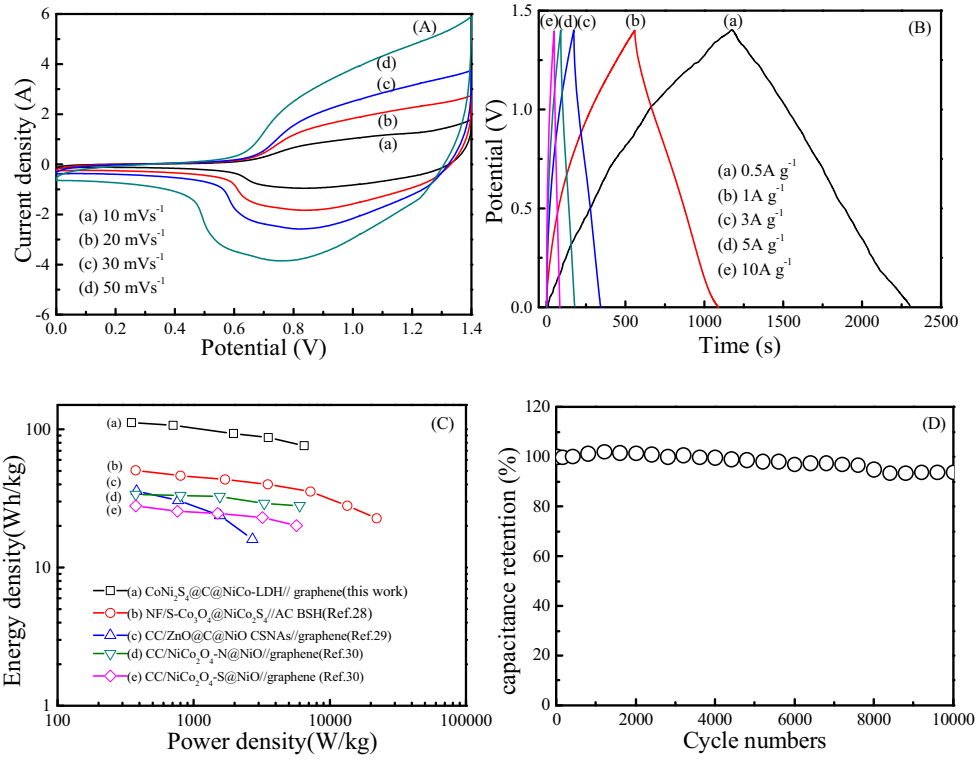

Fig. 8 CV plots at various scan rates (**A**), charge-discharge curves at successive current densities (**B**), relationship of energy and power densities with another device in literature (**C**), and cycling performances at a current density of 5 A g^{-1} (**D**) of the as-assembled $CoNi_2S_4$@C@NiCo-LDH//graphene asymmetric supercapacitor in 6 mol L^{-1} KOH electrolyte

increased from 1 to 10 A g^{-1}, the galvanostatic charge-discharge curves of the $CoNi_2S_4$@C@NiCo-LDH//graphene asymmetric supercapacitor retained their symmetrical triangle shape (Fig. 8B), manifesting a great electrochemical response at high current density. The specific capacitances of the evaluated asymmetric supercapacitor were calculated to be ca. 550, 479, 448, and 392 mAh g^{-1} at 1, 3, 5, and 10 A g^{-1}, exhibiting an exceptional rate capability of 71.3%. Furthermore, the assembled asymmetric supercapacitor shows an excellent energy density of 111.9 Wh kg^{-1}. As the power density increased from 349.1 to 6483.8 W kg^{-1}, the energy density of $CoNi_2S_4$@C@NiCo-LDH//graphene device was reduced from 111.9 to 76.14 Wh kg^{-1}, which are higher than many reported asymmetric supercapacitors, such as NF/S-Co_3O_4@$NiCo_2S_4$//AC BSH (50.5 Wh kg^{-1} at 375 W kg^{-1}) [27], CC/ZnO@C@NiO CSNAs//graphene (16.0 Wh kg^{-1} at 2704.2 W kg^{-1}) [28], CC/$NiCo_2O_4$-N@NiO//graphene (28 Wh kg^{-1} at 6000 W kg^{-1}), and CC/$NiCo_2O_4$-S@NiO//graphene (20.1 Wh kg^{-1} at 5692 W kg^{-1}) [29]. To investigate the cyclic stability of the assembled asymmetric supercapacitor, the galvanostatic charge-discharge experiments are performed at a current density of 5 A g^{-1} for 10,000 cycles in 6 mol L^{-1} KOH electrolyte. After continuous charge-discharge cycles, the specific capacitance value can retain 93.8% of the initial value (Fig. 8C). These good cycling life and electrochemical reversibility may be attributed to the intermediate carbon layer, which can not only enhance electrical conductivity but also provide much more attachment sites for $CoNi_2S_4$ and NiCo-LDH.

Conclusion

Hollow sandwich nanostructured $CoNi_2S_4$@C@NiCo-LDH nanocomposites were successfully designed and prepared by a convenient microwave-assisted hydrothermal method, which were utilized as efficient electrode materials for supercapacitors. The designed $CoNi_2S_4$@C@NiCo-LDH microspheres exhibited high specific capacitance, excellent cycle life, and fast charge-discharge response at high current densities. Furthermore, the assembled $CoNi_2S_4$@C@NiCo-LDH//graphene asymmetric supercapacitor could supply an eminent pseudocapacitance of 550 mAh g^{-1} and retain 93.8% of the initial value after consecutive 10,000 cycles. This work provided a novel and promising electrode material for future energy storage devices.

Funding information We gratefully thank the National Natural Science Foundation of China (Grant No. 21773018 and 21573025) and Natural Science Foundation of the Jiangsu Higher Education Institutions of China (Grant No. 17KJA150001) for support of this work.

References

1. Dong LB, Xu CJ, Li Y, Huang ZH, Kang FY, Yang QH, Zhao X (2016) Flexible electrodes and supercapacitors for wearable energy storage: a review by category. J Mater Chem A 4(13):4659–4685
2. Zhang L, Hu X, Wang Z, Sun F, Dorrell DG (2018) A review of supercapacitor modeling, estimation, and applications: a control/management perspective. Renew Sust Energ Rev 81:1868–1878
3. Xiong P, Zhu J, Wang X (2015) Recent advances on multi-component hybrid nanostructures for electrochemical capacitors. J Power Sources 294:31–50
4. Yan T, Li R, Zhou L, Ma C, Li Z (2015) Three-dimensional electrode of Ni/co layered double hydroxides@$NiCo_2S_4$@graphene@Ni foam for supercapacitors with outstanding electrochemical performance. Electrochim Acta 176:1153–1164
5. Hou Y, Cheng Y, Hobson T, Liu J (2010) Design and synthesis of hierarchical MnO_2 nanospheres/carbon nanotubes/conducting polymer ternary composite for high performance electrochemical electrodes. Nano Lett 10(7):2727–2733
6. Hu X, Jia J, Wang G, Chen J, Zhan H, Wen Z (2018) Reliable and general route to inverse opal structured nanohybrids of carbon-confined transition metal sulfides quantum dots for high-performance sodium storage. Adv Energy Mater 8(25):1801452
7. Wen P, Fan M, Yang D, Wang Y, Cheng H, Wang J (2016) An asymmetric supercapacitor with ultrahigh energy density based on nickle cobalt sulfide nanocluster anchoring multi-wall carbon nanotubes hybrid. J Power Sources 320:28–36
8. Bai Y, Wang WQ, Wang RR, Sun J, Gao L (2015) Controllable synthesis of 3D binary nickel-cobalt hydroxide/graphene/nickel foam as a binder-free electrode for high-performance supercapacitors. J Mater Chem A 3(23):12530–12538
9. Lin J, Zheng Y, Du Q, He M, Deng Z (2013) Synthesis and electrochemical properties of graphene/MnO_2/conducting polymer ternary composite for supercapacitors. Nano 8(01):1350004
10. Dubal DP, Ayyad O, Ruiz V, Gómez-Romero P (2015) Hybrid energy storage: the merging of battery and supercapacitor chemistries. Chem Soc Rev 44(7):1777–1790
11. Gao YP, Huang KJ (2017) $NiCo_2S_4$ materials for supercapacitor applications. Chem Asian J 12(16):1969–1984
12. Jagadale A, Zhou X, Blaisdell D, Yang S (2018) Carbon nanofibers (CNFs) supported cobalt-nickel sulfide ($CoNi_2S_4$) nanoparticles hybrid anode for high performance lithium ion capacitor. Sci Rep 8(1):1602
13. Pu J, Cui FL, Chu SB, Wang TT, Sheng EH, Wang ZH (2014) Preparation and electrochemical characterization of hollow hexagonal $NiCo_2S_4$ nanoplates as pseudocapacitor materials. ACS Sustain Chem Eng 2(4):809–815
14. Tang YF, Chen T, Yu SX, Qiao YQ, Mu SC, Zhang SH, Zhao YF, Hou L, Huang WW, Gao FM (2015) A highly electronic conductive cobalt nickel sulphide dendrite/quasi-spherical nanocomposite for a supercapacitor electrode with ultrahigh areal specific capacitance. J Power Sources 295:314–322
15. Xiong XH, Waller G, Ding D, Chen DC, Rainwater B, Zhao BT, Wang ZX, Liu ML (2015) Controlled synthesis of $NiCo_2S_4$ nanostructured arrays on carbon fiber paper for high-performance pseudocapacitors. Nano Energy 16:71–80
16. Hu W, Chen R, Xie W, Zou L, Qin N, Bao D (2014) $CoNi_2S_4$ nanosheet arrays supported on nickel foams with ultrahigh capacitance for aqueous asymmetric supercapacitor applications. ACS Appl Mater Inter 6(21):19318–19326
17. Shen J, Wu J, Pei L, Rodrigues MTF, Zhang ZQ, Zhang F, Zhang X, Ajayan PM, Ye M (2016) $CoNi_2S_4$-graphene-2D-$MoSe_2$ as an advanced electrode material for supercapacitors. Adv Energy Mater 6(13):1600341

18. Ai Z, Hu Z, Liu Y, Yao M (2016) Capacitance performance of nanostructured $CoNi_2S_4$ with different morphology grown on carbon cloth for supercapacitors. Chem Plus Chem 81:322–328
19. Du W, Wang Z, Zhu Z, Hu S, Zhu X, Shi Y, Pang H, Qian X (2014) Facile synthesis and superior electrochemical performances of $CoNi_2S_4$/graphene nanocomposite suitable for supercapacitor electrodes. J Mater Chem A 2(25):9613–9619
20. Peng SJ, Li LL, Li CC, Tan HT, Cai R, Yu H, Mhaisalkar S, Srinivasan M, Ramakrishna S (2013) In situ growth of $NiCo_2S_4$ nanosheets on graphene for high-performance supercapacitors. Chem Commun 49(86):10178–10180
21. Ai Z, Hu Z, Liu Y, Fan M, Liu P (2016) Novel 3D flower-like $CoNi_2S_4$/carbon nanotube composites as high-performance electrode materials for supercapacitors. New J Chem 40(1):340–347
22. Hou Y, Qiu S, Hu Y, Kundu CK, Gui Z, Hu W (2018) Construction of bimetallic ZIF-derived co-Ni LDHs on the surfaces of GO or CNTs with a recyclable method: toward reduced toxicity of gaseous thermal decomposition products of unsaturated polyester resin. ACS Appl Mater Inter 10(21):18359–18371
23. Daud M, Kamal MS, Shehzad F, Al-Harthi MA (2016) Graphene/layered double hydroxides nanocomposites: a review of recent progress in synthesis and applications. Carbon 104:241–252
24. Xu J, Dong YZ, Cao JY, Guo B, Chang WC, Chen ZD (2013) Microwave-incorporated hydrothermal synthesis of urchin-like $Ni(OH)_2$-$co(OH)_2$ hollow microspheres and their supercapacitor applications. Electrochim Acta 114:76–82
25. Nagaraju G, Raju GSR, Ko YH, Yu JS (2016) Hierarchical Ni-Co layered double hydroxide nanosheets entrapped on conductive textile fibers: a cost-effective and flexible electrode for high-performance pseudocapacitors. Nanoscale 8(2):812–825
26. Shen LF, Yu L, Wu HB, Yu XY, Zhang XG, Lou XW (2015) Formation of nickel cobalt sulfide ball-in-ball hollow spheres with enhanced electrochemical pseudocapacitive properties. Nat Commun 6:7694
27. Ouyang Y, Ye HT, Xia XF, Jiao XY, Li GM, Mutahir S, Wang L, Mandler D, Lei W, Hao QL (2019) Hierarchical electrodes of $NiCo_2S_4$ nanosheets anchored sulfur-doped Co_3O_4 nanoneedles with advanced performance for battery-supercapacitor hybrid devices. J Mater Chem A 7(7):3228–3237. https://doi.org/10.1039/C8TA11426A
28. Ouyang Y, Xia XF, Ye HT, Wang L, Jiao XY, Lei W, Hao QL (2018) Three-dimensional hierarchical structure ZnO@C@NiO on carbon cloth for asymmetric supercapacitor with enhanced cycle stability. ACS Appl Mater Inter 10(4):3549–3561
29. Ouyang Y, Huang RJ, Xia XF, Ye HT, Jiao XY, Wang L, Lei W, Hao QL (2019) Hierarchical structure electrodes of NiO ultrathin nanosheets anchored to $NiCo_2O_4$ on carbon cloth with excellent cycle stability for asymmetric supercapacitors. Chem Eng J 355:416–427
30. Liu X, Shi S, Xiong Q, Li L, Zhang Y, Tang H, Gu C, Wang X, Tu J (2013) Hierarchical $NiCo_2O_4$@$NiCo_2O_4$ core/shell nanoflake arrays as high-performance supercapacitor materials. ACS Appl Mater Interfaces 5(17):8790–8795
31. Wan L, Xiao J, Xiao F, Wang S (2014) Nanostructured (Co, Ni)-based compounds coated on a highly conductive three dimensional hollow carbon nanorod array (HCNA) scaffold for high performance pseudocapacitors. ACS Appl Mater Interfaces 6(10):7735–7742
32. Peng HH, Chen J, Jiang DY, Guo XL, Chen H, Zhang YX (2016) Merging of memory effect and anion intercalation: MnO_x-decorated MgAl-LDO as a high-performance nano-adsorbent for the removal of methyl orange. Dalton Trans 45(26):10530–10538
33. Tang JH, Shen JF, Li N, Ye MX (2015) One-pot tertbutanol assisted solvothermal synthesis of $CoNi_2S_4$/reduced graphene oxide nanocomposite for high-performance supercapacitors. Ceram Int 41(5):6203–6211
34. Li M, Cheng JP, Liu F, Zhang XB (2015) In situ growth of nickel-cobalt oxyhydroxide/oxide on carbon nanotubes for high performance supercapacitors. Electrochim Acta 178:439–446
35. Lv YY, Zhang F, Dou YQ, Zhai YP, Wang JX, Liu HJ, Xia YY, Tu B, Zhao DY (2012) A comprehensive study on KOH activation of ordered mesoporous carbons and their supercapacitor application. J Mater Chem A 22(1):93–99
36. Chen W, Xia C, Alshareef HN (2014) One-step electrodeposited nickel cobalt sulfide nanosheet arrays for high-performance asymmetric supercapacitors. ACS Nano 8(9):9531–9541
37. Jing MJ, Yang YY, Zhu YR, Hou HS, Wu ZB, Ji XB (2014) An asymmetric ultracapacitors utilizing α-$Co(OH)_2$/Co_3O_4 flakes assisted by electrochemically alternating voltage. Electrochim Acta 141:234–240
38. Gao Y, Mi LW, Wei WT, Cui SZ, Zheng Z, Hou HW, Chen WH (2015) Double metal ions synergistic effect in hierarchical multiple sulfide microflowers for enhanced supercapacitor performance. ACS Appl Mater Inter 7(7):4311–4319
39. Xu J, Ju Z, Cao J, Wang W, Wang C, Chen Z (2016) Microwave synthesis of nitrogen-doped mesoporous carbon/nickel-cobalt hydroxide microspheres for high-performance supercapacitors. J Alloys Compd 689:489–499